Eur. J. Mineral.
2018, **30**, 801–809
Published online 4 May 2018

Calamaite, a new natural titanium sulfate from the Alcaparrosa mine, Calama, Antofagasta region, Chile

IGOR V. PEKOV[1,2,*], OLEG I. SIIDRA[3,4], NIKITA V. CHUKANOV[5], VASILIY O. YAPASKURT[1], DMITRY I. BELAKOVSKIY[6], ANNA G. TURCHKOVA[1] and GERHARD MÖHN[7]

[1] Faculty of Geology, Moscow State University, Vorobievy Gory, 119991 Moscow, Russia
*Corresponding author, e-mail: igorpekov@mail.ru
[2] Institute of Geochemistry and Analytical Chemistry, Kosygin str. 19, 117975 Moscow, Russia
[3] Department of Crystallography, St Petersburg State University, Universitetskaya Nab. 7/9, 199034 St Petersburg, Russia
[4] Nanomaterials Research Center, Kola Science Center, Russian Academy of Sciences, Apatity, Murmansk Region, 184200, Russia
[5] Institute of Problems of Chemical Physics, Russian Academy of Sciences, 142432 Chernogolovka, Moscow region, Russia
[6] Fersman Mineralogical Museum of Russian Academy of Sciences, Leninsky Prospekt 18-2, 119071 Moscow, Russia
[7] Dr.-J.-Wittemannstrasse 5, 65527 Niedernhausen, Germany

Abstract: The new mineral calamaite, $Na_2TiO(SO_4)_2 \cdot 2H_2O$, was found in the oxidation zone of a pyrite orebody at the abandoned Alcaparrosa sulfate mine, Calama commune, El Loa province, Antofagasta region, Chile. It is associated with römerite, coquimbite, metavoltine, tamarugite, halotrichite, szomolnokite, rhomboclase, and ferricopiapite. Calamaite forms acicular to hair-like crystals up to 0.01×2 mm combined in bunches or radial spherulitic clusters up to 4 mm across; rarely prismatic crystals up to $1 \times 1 \times 3$ mm occur. Cross-like interpenetration twins are common. Calamaite is transparent, colourless in separate crystals and white in aggregates, with vitreous lustre. The mineral is brittle, with Mohs' hardness *ca*. 3. Good cleavage, presumably on (0 0 1), was observed. D_{calc} is 2.45 g · cm^{-3}. Calamaite is optically biaxial (+), $\alpha = 1.557(2)$, $\beta = 1.562(2)$, $\gamma = 1.671(3)$, $2V_{meas} = 30(10)°$. The IR spectrum is reported. The chemical composition (wt%, electron microprobe data; H_2O content is calculated for $2H_2O$ pfu) is: Na_2O 18.21, K_2O 0.06, Fe_2O_3 1.58, TiO_2 21.80, SO_3 48.25, H_2O_{calc} 10.74, total 100.73. The empirical formula calculated on the basis of 11 O apfu is: $Na_{1.97}(Ti_{0.92}Fe^{3+}_{0.07})_{\Sigma 0.99}S_{2.02}O_9 \cdot 2_{H2O}$ Calamaite is orthorhombic, *Ibam*, $a = 16.0989(11)$, $b = 16.2399(9)$, $c = 7.0135(4)$ Å, $V = 1833.6(2)$ Å^3, and $Z = 8$. The strongest reflections of the powder XRD pattern [*d*,Å(*I*)(*hkl*)] are: 8.10(1 0 0)(0 2 0, 2 0 0), 5.04(55)(1 2 1, 2 1 1), 3.787(26)(2 3 1), 3.619(18)(2 4 0, 4 2 0), 3.417(27)(1 4 1, 4 1 1), 3.185(15)(1 5 0), 2.943(20)(3 4 1, 4 3 1), and 2.895(20)(1 3 2, 3 1 2). Calamaite represents a novel structure type. Its crystal structure was solved from single-crystal XRD data ($R = 0.0358$). The TiO_6 octahedra are interconnected *via* O vertices to form infinite $(Ti–O)_\infty$ chains. The remaining vertices of each TiO_6 octahedron are shared with SO_4 tetrahedra thus forming one-dimensional $[TiO(SO_4)_2]$ units. Cohesion of the $[TiO(SO_4)_2]$ units into framework is provided *via* two crystallographically independent Na atoms. The mineral is named after the Calama commune and the Calama city (IMA2016-036).

Key-words: calamaite; new mineral; titanium sulfate; crystal structure; oxidation zone; Alcaparrosa mine; El Loa; province; Chile.

1. Introduction

Titanium is one of the very significant chemical elements in geochemistry. It is an essential constituent of many important accessory minerals of magmatic, metamorphic and metasomatic rocks and a typical minor or, less commonly, even species-defining element of some rock-forming minerals. The mineralogy of titanium is diverse: *ca*. three hundreds valid minerals with species-defining Ti^{4+} are now known. They demonstrate a strongly uneven distribution among chemical classes: the overwhelming majority belongs to silicates (*ca*. 190 mineral species) and oxides and hydroxides (*ca*. 90). Among two dozens of Ti minerals not belonging to these classes (all are extremely rare in nature), seven are oxygen-free species (mainly known in meteorites) while the others are oxysalts, including three phosphates, three arsenites, three arsenates, one carbonate, one borate, one tellurite, and one sulfate. The last one listed is alcaparrosaite recently discovered at the Alcaparrosa mine in Northern Chile. Its

0935-1221/18/0030-2738 $ 4.05
https://doi.org/10.1127/ejm/2018/0030-2738

idealized formula was written as $K_3TiFe^{3+}(SO_4)_4O \cdot 2H_2O$, however, Ti^{4+} and Fe^{3+} are disordered at the same structural position being in nearly equal amounts (Kampf *et al.*, 2012), consequently, the crystal chemical formula of alcaparrosaite is in fact $K_3(Ti^{4+}_{0.5}Fe^{3+}_{0.5})_2(SO_4)_4O{\cdot}2H_2O$.

In the present paper we describe the new mineral calamaite, ideally $Na_2TiO(SO_4)_2 \cdot 2H_2O$, the second natural titanium sulfate. It was found at the same Alcaparrosa mine. Unlike alcaparrosaite, the new mineral is characterized by a strong predominance of Ti at one structural site. Calamaite (Cyrillic: каламаит) is named after the Calama commune, in which its type locality is situated, and the Calama city, the capital of El Loa province. This area is famous in both mining and mineralogical aspects due to the location of outstanding ore deposits, mainly of copper, with very rich and interesting supergene mineralization in the oxidation zone. Both the new mineral and its name have been approved by the IMA Commission on New Minerals, Nomenclature and Classification (IMA2016-036). The type specimen is deposited in the systematic collection of the Fersman Mineralogical Museum of the Russian Academy of Sciences, Moscow, with the catalogue number 95619.

2. Occurrence

The abandoned Alcaparrosa sulfate mine is situated at the north side of Cerro Alcaparrosa, about 3 km southwest of the railroad station of Cerritos Bayos, Calama commune, El Loa province, Antofagasta region, Chile. The Alcaparrosa deposit contains veins and lenses consisting of diverse iron sulfates and formed as a result of the oxidation of pyrite ore under the extremely arid conditions of the Atacama Desert. The pyrite-rich orebodies are located in volcanic rocks of the Punta del Cobre Formation mainly consisting of andesites and dacites (Marschik & Fontboté, 2001). The mine was intermittently in operation between 1875 and 1920, mainly for römerite and coquimbite as a raw material for sulfuric acid. Due to the absence of copper or other commercially profitable metals, the Alcaparrosa deposit had low economic value (Bandy, 1938); however, it is famous as a mineralogical object, a source of numerous museum-quality specimens of many iron sulfates. Alcaparrosa is the type locality of five sulfates: two "grandfathered" species, paracoquimbite and parabutlerite (Palache *et al.*, 1951), and three minerals discovered recently, namely alcaparrosaite (Kampf *et al.*, 2012), magnesiovoltaite, $K_2Mg_5Fe^{3+}{}_3Al(SO_4)_{12} \cdot 18H_2O$ (Chukanov *et al.*, 2016a), and calamaite.

Specimens with calamaite were collected by us in January 2016 in an old underground working at the upper part of the mine. Calamaite was found in a römerite-enriched cavernous zone located inside a sulfate body mainly composed by coquimbite. Numerous cracks and cavities in a massive ferricopiapite–römerite–coquimbite rock are encrusted here with coquimbite and römerite crystal crusts. Other minerals found here are metavoltine, tamarugite, halotrichite, szomolnokite, rhomboclase and, in minor amounts, ferrinatrite, krausite, and calamaite. The supergene mineralization

a

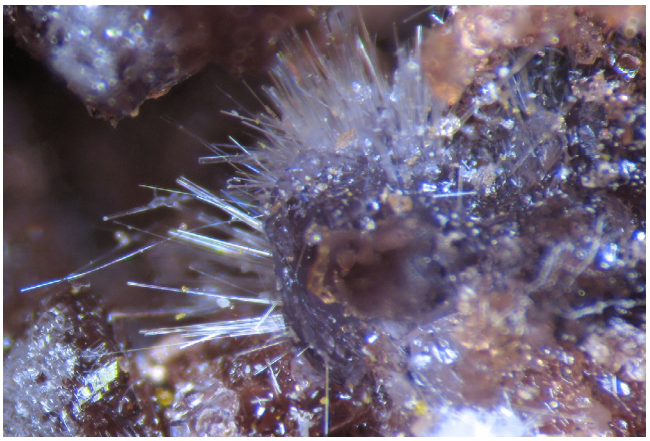

b

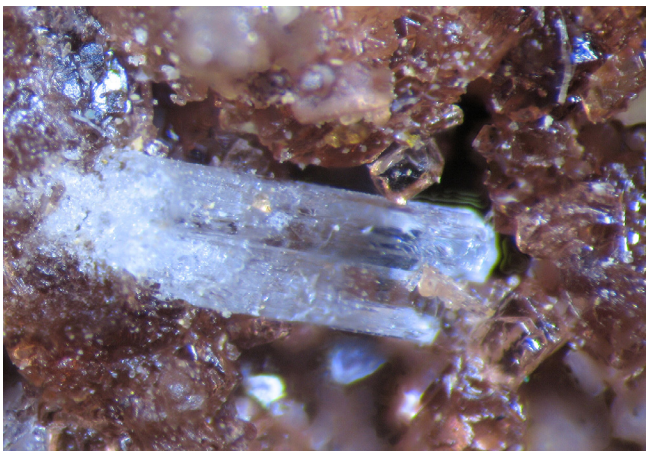

c

Fig. 1. Morphology of crystals and aggregates of calamaite: (a) white radial spherulitic cluster consisting of acicular to hair-like crystals on red-brown römerite crystal crust with mustard-yellow metavoltine crystals; (b) colourless acicular crystals penetrating a lilac crystal of coquimbite on red-brown römerite crystal crust; (c) colourless, transparent prismatic crystal on red-brown römerite crystals. Field of view: (a) 3.8 mm; (b) 4.0 mm; (c) 2.8 mm. Photo: A.V. Kasatkin & I.V. Pekov.

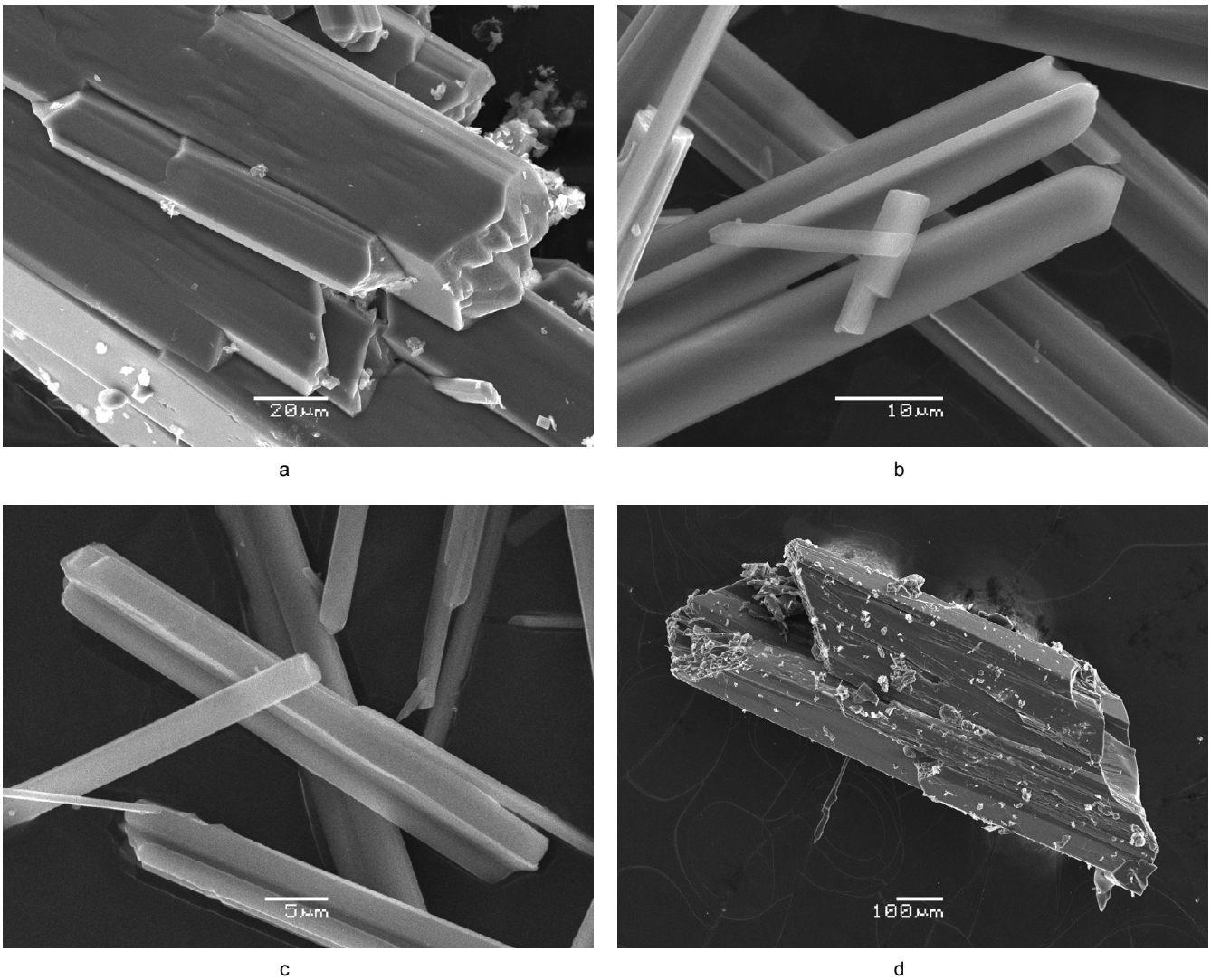

Fig. 2. Crystal morphology of calamaite: (a) prismatic crystals with coarse terminations; (b) sword-like single crystal and cross-like interpenetration twin; (c) cross-like interpenetration twins; (d) skeletal, case-like crystal. SEM (SE) image.

observed by us in this underground working also includes magnesiocopiapite, copiapite, butlerite, parabutlerite, voltaite, pertlikite, alcaparrosaite, alunogene, natrojarosite, gypsum, lesukite, and opal. Pyrite, quartz, plagioclase, and rutile are relict minerals. Native sulfur occurs as a product of the first step of supergene alteration of pyrite.

Calamaite occurs in cavities of open-work sulfate aggregates mainly consisting of red-brown römerite. The new mineral overgrows römerite or forms intimate intergrowths with it, as well as with coquimbite and metavoltine (Fig. 1).

3. General appearance, physical properties and optical data

Calamaite typically forms thin, acicular to hair-like crystals up to 2 mm long and up to 0.01 mm thick combined in bunches or radial spherulitic clusters (Fig. 1a) up to 4 mm in diameter. Thicker (up to 1.5 mm long and up to 0.05 mm thick) needles and their groups (Fig. 1b) occur less frequently. The rarest morphological variety of calamaite is represented by isolated prismatic crystals up to $1 \times 1 \times 3$ mm (Fig. 1c). Calamaite crystals are elongated along [0 0 1]. Most of them are poorly terminated (Fig. 2a); however, some thin crystals have sword-like terminations (Fig. 2b). Crystal faces were not indexed; we assume that the main crystal forms are pinacoids {1 0 0} and {0 1 0}. Cross-like interpenetration twins are common (Fig. 2b and c). They are rotation twins with the rotation axis [0 0 1] and a rotation angle of 90°. The thickest crystals are typically skeletal, case-like (Fig. 2d).

Calamaite is transparent, colourless in separate crystals and white in aggregates. Its lustre is vitreous. The mineral is non-fluorescent under ultraviolet light or an electron beam. Calamaite is brittle. Its Mohs' hardness is *ca*. 3. One plane of good cleavage was observed under the microscope, presumably on (100) (the plane is assumed based on the structure data). The fracture is uneven; for some grains

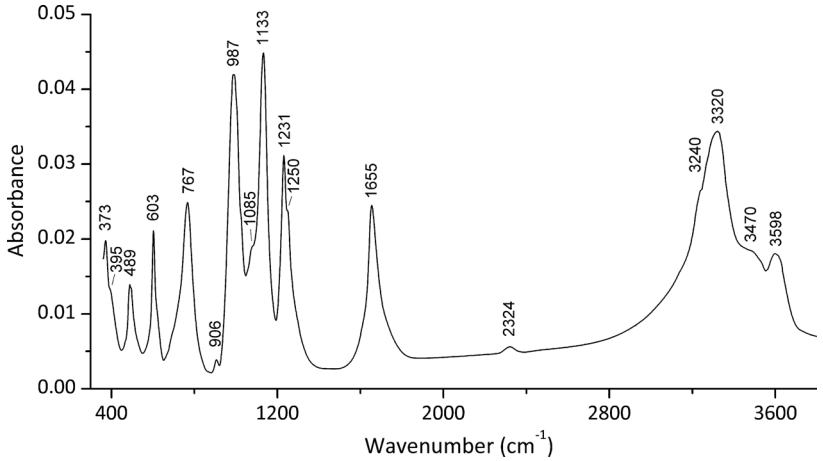

Fig. 3. IR absorption spectrum of calamaite.

Table 1. Powder X-ray diffraction data of calamaite.

I_{obs}	d_{obs}	I_{calc}*	d_{calc}**	*h k l*
0.5	11.48	0.5	11.433	1 1 0
100	8.10	100, 88	8.120, 8.045	0 2 0, 2 0 0
0.5	5.72	0.5	5.717	2 2 0
55	5.04	81, 15	5.041, 5.028	1 2 1, 2 1 1
6	4.056	4, 3	4.060, 4.025	0 4 0, 4 0 0
26	3.787	44	3.783	2 3 1
18	3.619	14, 18	3.625, 3.606	2 4 0, 4 2 0
5	3.509	8	3.507	0 0 2
27	3.417	2, 44	3.433, 3.413	1 4 1, 4 1 1
12	3.219	11, 10	3.219, 3.215	0 2 2, 2 0 2
15	3.185	20	3.184	1 5 0
13	3.164	17	3.158	5 1 0
9	2.992	21	2.989	2 2 2
20	2.943	30, 4	2.940, 2.934	3 4 1, 4 3 1
20	2.895	27, 21	2.895, 2.889	1 3 2, 3 1 2
2	2.862	2	2.858	4 4 0
14	2.777	15, 0.5, 12	2.779, 2.768, 2.767	3 5 0, 2 5 1, 5 3 0
6	2.709	8	2.707	0 6 0
5	2.687	7	2.683	6 0 0
7	2.652	10	2.654	0 4 2
2	2.570	2	2.565	2 6 0
3	2.551	4	2.548	6 2 0
5	2.521	8	2.520	2 4 2
5	2.480	8	2.477	6 1 1
2	2.358	5	2.357	1 5 2
3	2.299	3	2.296	1 7 0
5	2.287	7	2.285	3 6 1
5	2.218	11	2.216	4 4 2
2	2.176	1, 3	2.178, 2.172	3 5 2, 5 3 2
3	2.143	5	2.143	0 6 2
3	2.134	5	2.131	6 0 2
1	2.119	1, 2	2.125, 2.117	2 7 1, 7 3 0
5	2.072	2, 9	2.072, 2.071	3 2 3, 2 6 2
4	2.065	6	2.061	6 2 2
2	2.032	3	2.030	0 8 0
3	2.011	3, 3, 4	2.012, 2.010, 2.006	8 0 0, 1 4 3, 4 1 3
4	1.971	8	1.968	2 8 0
5	1.956	10	1.953	8 2 0
0.5	1.935	0.5, 0.5	1.936, 1.932	1 8 1, 4 7 1
1	1.927	2	1.924	7 4 1
2	1.907	4	1.906	6 6 0
3	1.896	5	1.895	3 4 3
2	1.848	5	1.847	2 5 3
1	1.835	2	1.833	3 8 1
2	1.814	3	1.812	4 8 0

Table 1. (continued).

I_{obs}	d_{obs}	I_{calc} *	d_{calc} **	*h k l*
3	1.806	6	1.803	8 4 0
1	1.796	2	1.793	1 9 0
0.5	1.780	1	1.778	9 1 0
6	1.756	6, 15, 1	1.757, 1.753, 1.752	0 8 2, 0 0 4, 6 1 3
2	1.747	5	1.745	8 0 2
2	1.718	4, 0.5	1.716, 1.716	2 8 2, 4 5 3
1	1.708	3	1.706	8 2 2
1	1.698	2	1.695	9 2 1
3	1.676	9	1.674	6 6 2
1	1.658	0.5, 2	1.658, 1.655	5 7 2, 7 5 2
1	1.613	1	1.613	2 7 3
1	1.606	2	1.603	4 9 1
1	1.588	2	1.586	9 1 2
3	1.579	4, 5	1.578, 1.577	2 4 4, 4 2 4
1	1.508	4	1.506	4.1 0.0
2	1.498	5, 3	1.497, 1.495	10.4.0, 4 4 4
3	1.474	9	1.474	0.10.2
2	1.466	3, 1, 3, 7	1.470, 1.468, 1.467, 1.463	6 8 2, 6 0 4, 8 6 2, 10.0.2
1	1.419	1, 1, 4	1.422, 1.420, 1.417	2.11.1, 7 9 0, 9 7 0
1	1.379	0.5, 2, 1	1.380, 1.377, 1.376	6 4 4, 125, 10.4.2
1	1.352	2, 1, 3	1.354, 1.353, 1.350	3 7 4, 0.12.0, 7 3 4
1	1.321	0.5, 2	1.322, 1.320	10.1.3, 4 1 5
1	1.294	5	1.292	6.10.2
2	1.289	2, 1, 2, 5	1.290, 1.288, 1.287, 1.287	6 6 4, 10.3.3, 345, 10.6.2
1	1.263	2, 2, 1, 1	1.264, 1.261, 1.261, 1.260	8.10.0, 10.8.0, 6 9 3, 4 8 4

* For the calculated pattern, only reflections with intensities ≥0.5 are given.
** For the unit-cell parameters calculated from single-crystal data.

stepped fracture was observed under the microscope. Density was not measured because solid crystals (without cavities) are too thin, whereas the thickest crystals are case-like (Fig. 2d). The density calculated using the empirical formula is 2.45 $g \cdot cm^{-3}$.

In plane-polarized light calamaite is colourless and non-pleochroic. It is optically biaxial (+), $\alpha = 1.557(2)$, $\beta = 1.562(2)$, $\gamma = 1.671(3)$ (589 nm). $2V_{meas} = 30(10)°$ and $2V_{calc} = 25°$. Dispersion of optical axes was not observed. Orientation: *XZ* is coplanar to the cleavage plane; if the cleavage plane is (1 0 0) (see above) then $Y = a$. Extinction is straight and elongation is positive.

4. Infrared spectroscopy

In order to obtain an infrared (IR) absorption spectrum (Fig. 3), a powdered sample of calamaite was mixed with dried KBr, pelletized, and analyzed using an ALPHA FTIR spectrometer (Bruker Optics) with a resolution of 4 cm^{-1} and 16 scans. The IR spectrum of an analogous pellet of pure KBr was used as a reference.

Wavenumbers of absorption bands in the IR spectrum of calamaite and their assignments (cm^{-1}; s – strong band, w – weak band, sh – shoulder) are: 3598, 3470sh, 3320s, 3240sh [O–H stretching vibrations of H_2O molecules and minor OH^- groups substituting O^{2-} at the O(1) site], 2324 w [combination mode of S–O stretching vibrations], 1655 [bending vibrations of H_2O molecules], 1250sh, 1231s, 1133s, 1085sh [$\nu_3(F_2)$ – asymmetric stretching vibrations of SO_4^{2-}anions], 987s [$\nu_1(A_1)$ – symmetric

Table 2. Crystal data and data collection and structure refinement details for calamaite.

Crystal data	
Crystal system	orthorhombic
Space group	*Ibam*
Unit cell dimensions	
a (Å)	16.0989(11)
b (Å)	16.2399(9)
c (Å)	7.0135(4)
Unit-cell volume (Å^3)	1833.64(19)
Z	8
Calculated density ($g \cdot cm^{-3}$)	2.45
Absorption coefficient (mm^{-1})	1.533
Crystal size (mm)	0.12 × 0.12 × 0.08
Data collection	
Temperature (K)	296(2)
Radiation, wavelength (Å)	Mo*K*α, 0.71073
F(0 0 0)	1312
θ range (°)	1.781–27.982
h, *k*, *l* ranges	–21→18, –21→21, –9→8
Total reflections collected	10290
Unique reflections (R_{int})	1205 (0.01)
Unique reflections $F > 4\sigma(F)$	1185
Structure refinement	
Refinement method	Full-matrix least-squares on F^2
Weighting coefficients *a*, *b*	0.032000, 10.129805
Data/restraints/parameters	1205/0/91
R_1 [$F > 4\sigma(F)$], wR_2 [$F > 4\sigma(F)$]	0.0358, 0.0941
R_2 all, wR_2 all	0.0362, 0.0937
Gof on F^2	1.237
Largest diff. peak, hole ($e \cdot$ Å^{-3})	0.601, –0.963

Table 3. Atom coordinates and displacement parameters (U, Å^2) and bond-valence sums (*B.V.S.*) for calamaite.

Site	*B.V.S.*	x	y	z	U_{eq}
Ti*	4.08	¼	¼	¼	0.0283(3)
Na(1)	0.99	0	0.16179(12)	¼	0.0357(5)
Na(2)	0.97	0.33838(12)	0	¼	0.0371(5)
S(1)	6.04	0.19001(5)	0.09112(5)	0	0.0140(2)
S(2)	6.01	0.41140(5)	0.19584(5)	0	0.0144(2)
O(1)**	1.58	0.22607(17)	0.28840(16)	0	0.0162(5)
O(2)	1.93	0.22911(19)	0.01076(17)	0	0.0224(6)
O(3)	2.01	0.36719(11)	0.22832(13)	0.1728(3)	0.0209(4)
O(4)	1.96	0.49434(17)	0.23073(18)	0	0.0220(6)
O(5)	2.04	0.21989(13)	0.13621(11)	0.1730(3)	0.0224(4)
O(6)	1.79	0.4102(2)	0.10695(18)	0	0.0313(7)
O(7)	1.82	0.10026(19)	0.0880(2)	0	0.0308(7)
OW(8)	0.36	0.0783(2)	0.0923(2)	½	0.0324(8)
OW(9)	0.42	0.1012(2)	0.4205(2)	0	0.0343(8)

Site	U_{11}	U_{22}	U_{33}	U_{23}	U_{13}	U_{12}
Ti*	0.0076(18)	0.0076(14)	0.0083(16)	0.0026(10)	0.0019(11)	0.0013(11)
Na(1)	0.0054(17)	0.0086(14)	0.0095(16)	0.0036(11)	0.0018(11)	−0.0007(11)
Na(2)	0.016(2)	0.0256(19)	0.0074(17)	0.0063(13)	0.0043(14)	0.0147(15)
S(1)	0.0059(14)	0.0071(11)	0.0045(12)	0.0010(9)	−0.0007(10)	0.0008(10)
S(2)	0.0039(14)	0.0068(11)	0.0038(12)	0.0027(9)	0.0011(9)	−0.0007(10)
O(1)**	0.0089(15)	0.0141(13)	0.0071(13)	0.0045(10)	0.0027(11)	−0.0002(11)
O(2)	0.010(6)	0.006(5)	0.011(5)	0.005(4)	0.002(4)	0.001(4)
O(3)	0.018(7)	0.008(5)	0.020(6)	0.008(4)	0.004(5)	−0.002(5)
O(4)	0.008(6)	0.010(5)	0.016(6)	0.000(4)	0.005(5)	−0.003(4)
O(5)	0.014(6)	0.023(6)	0.008(5)	0.011(5)	0.000(5)	0.010(5)
O(6)	0.006(6)	0.018(5)	0.009(5)	0.008(4)	−0.001(4)	−0.001(5)
O(7)	0.012(6)	0.015(5)	0.015(6)	0.008(4)	0.005(5)	0.006(5)
OW(8)	0.007(6)	0.012(5)	0.007(5)	0.003(4)	−0.004(4)	−0.003(4)
OW(9)	0.018(7)	0.026(6)	0.010(6)	0.011(5)	0.006(5)	0.000(5)

* Refined as $(Ti_{0.95}Fe_{0.05})$.
** Refined as $(O_{0.95}OH_{0.05})$. Bond-valence sums were calculated using the parameters from Brese & O'Keeffe (1991).

Table 4. Selected interatomic distances (Å) in the structure of calamaite.

Ti–O(1)	1.9004(10) × 2	S(1)–O(7)	1.446(3)
Ti–O(5)	1.9853(18) × 2	S(1)–O(2)	1.449(3)
Ti–O(3)	1.9943(18) × 2	S(1)–O(5)	1.497(2) × 2
⟨Ti–O⟩	1.960	⟨S–O⟩	1.472
Na(1)–OW(8)	2.437(2) × 2	S(2)–O(6)	1.444(3)
Na(1)–O(4)	2.476(3) × 2	S(2)–O(4)	1.451(3)
Na(1)–O(7)	2.667(3) × 2	S(2)–O(3)	1.5009(19) × 2
Na(1)–O(3)	2.837(2) × 2	⟨S–O⟩	1.474
⟨Na–O⟩	2.604		
Na(2)–OW(9)	2.385(2) × 2		
Na(2)–O(2)	2.490(3) × 2		
Na(2)–O(6)	2.726(3) × 2		
Na(2)–O(5)	2.970(2) × 2		
⟨Na–O⟩	2.643		

stretching vibrations of SO_4^{2-} anions], 906w [possibly, (Ti, Fe^{3+})···O–H bending vibrations], 767 [Ti–O-stretching vibrations involving short bonds Ti–O(1) along octahedral chains], 603 [$\nu_4(F_2)$ – bending vibrations of SO_4^{2-}anions], 489 [ν_2(E) bending mode of SO_4^{2-} anions combined with Ti–O-stretching vibrations in Ti–O–S bridges with longer Ti–O(3) and Ti–O(5) bonds], 395sh, 373 [mixed lattice modes involving O–Ti–O bending vibrations].

The presence of a strong band of symmetric S–O stretching vibrations of SO_4^{2-} anions (at 987 cm^{-1}) and the splitting of a band corresponding to the asymmetric stretching vibrations of SO_4^{2-}anions (in the range 1080–1250 cm^{-1}) confirm that calamaite contains strongly distorted SO_4 tetrahedra (for details see crystal-structure description).

The IR spectrum of calamaite is unique and may be used as good diagnostic tool of the mineral. Bands corresponding to BO_3^{3-}, CO_3^{2-} and NO_3^- (in the range 1260–1600 cm^{-1}) are absent in the IR spectrum of calamaite.

5. Chemical data

The chemical composition of calamaite was studied using a Jeol JSM-6480LV scanning electron microscope equipped with an INCA-Wave 500 wavelength-dispersive spectrometer (Laboratory of Analytical Techniques of High Spatial Resolution, Dept. of Petrology, Moscow State University), with an acceleration voltage of 20 kV,

a beam current of 20 nA, and a 3 μm beam diameter. The following standards were used: albite (Na), microcline (K), magnetite (Fe), ilmenite (Ti), GaP (P), and ZnS (S). Contents of other elements with atomic numbers higher than oxygen are below their detection limits. H_2O was not analysed because of paucity of available material; its content was calculated for $2H_2O$ pfu, based on the structure data (see below). Iron is assumed to be Fe^{3+} taking into account the results of chemical tests with $K_3Fe^{3+}(CN)_6$ and $K_4Fe^{2+}(CN)_6$ (see below). This assumption is in agreement with significantly oxidizing conditions of mineral formation: sulfates with only trivalent iron or with $Fe^{3+} > Fe^{2+}$ strongly prevail there.

The chemical composition of calamaite (average of 8 spot analyses; wt%, ranges in parentheses) is: Na_2O 18.21 (16.02–20.79), K_2O 0.06 (0.02–0.11), Fe_2O_3 1.58 (1.20–2.33), TiO_2 21.80 (20.95–23.59), SO_3 48.25 (47.30–49.66), H_2O_{calc} 10.74, total 100.73.

The empirical formula calculated on the basis of 11 O apfu is: $Na_{1.97}(Ti_{0.92}Fe^{3+}_{0.07})\sum_{0.99}S_{2.02}O_9 \cdot 2H_2O$. The idealized formula is $Na_2TiO(SO_4)_2 \cdot 2H_2O$ which requires Na_2O 18.34, TiO_2 23.64, SO_3 47.36, H_2O 10.66, total 100.00 wt%.

The Gladstone-Dale compatibility index is: $1-(K_p/K_c) = 0.008$, superior.

Calamaite is hardly soluble in H_2O at room temperature; however, the surface of its crystals turns white and dull if exposed to cold water for a day.

The presence of Fe^{3+} and absence of Fe^{2+} in calamaite were confirmed using well-known colour reactions with potassium hexaferricyanide, $K_3Fe^{3+}(CN)_6$, and potassium hexaferrocyanide, $K_4Fe^{2+}(CN)_6$. We observe blue colouring with $K_4Fe^{2+}(CN)_6$, which is a clear indicator of the presence of Fe^{3+}: $K_4Fe^{2+}(CN)_6 + Fe^{3+} \rightarrow$ blue $KFe^{2+}Fe^{3+}(CN)_6$, whereas no blue colouring appears in the test with $K_3Fe^{3+}(CN)_6$, which demonstrates the absence of Fe^{2+}: no sign of the reaction $K_3Fe^{3+}(CN)_6 + Fe^{2+} \rightarrow$ blue $KFe^{2+}Fe^{3+}(CN)_6$.

6. X-ray crystallography and crystal-structure description

Powder X-ray diffraction data of calamaite (Table 1) were collected with a Rigaku R-AXIS Rapid II single-crystal diffractometer equipped with cylindrical image-plate detector using Debye-Scherrer geometry (Co$K\alpha$ radiation, $d = 127.4$ mm). The data were integrated using the software package Osc2Tab (Britvin *et al.*, 2017). The orthorhombic unit-cell parameters refined from the powder data are: $a = 16.123(6)$, $b = 16.246(4)$, $c = 7.018(1)$ Å and $V = 1838(1)$ Å^3.

Single-crystal X-ray analysis of calamaite was carried out using a Bruker SMART diffractometer equipped with an APEX II CCD detector operating with Mo$K\alpha$ radiation at 50 kV and 40 mA. A single crystal with dimensions of $0.08 \times 0.12 \times 0.12$ mm was chosen for X-ray diffraction data. More than a hemisphere of data were collected with a frame width of 0.5° in ω, and 10 s spent counting for each frame. The data were integrated and corrected for absorption using a multi-scan type model using the Bruker programs APEX and SADABS (Bruker-AXS, 2014). Calamaite is orthorhombic, space group *Ibam*, $a = 16.0989(11)$, $b = 16.2399(9)$, $c = 7.0135(4)$ Å, $V = 1833.64(19)$ Å^3 and $Z = 8$ (Table 2). The structure was successfully refined using the SHELX software package (Sheldrick, 2015). Atom coordinates, bond-valence sums and displacement parameters for calamaite are given in Table 3 and selected interatomic distances in Table 4.

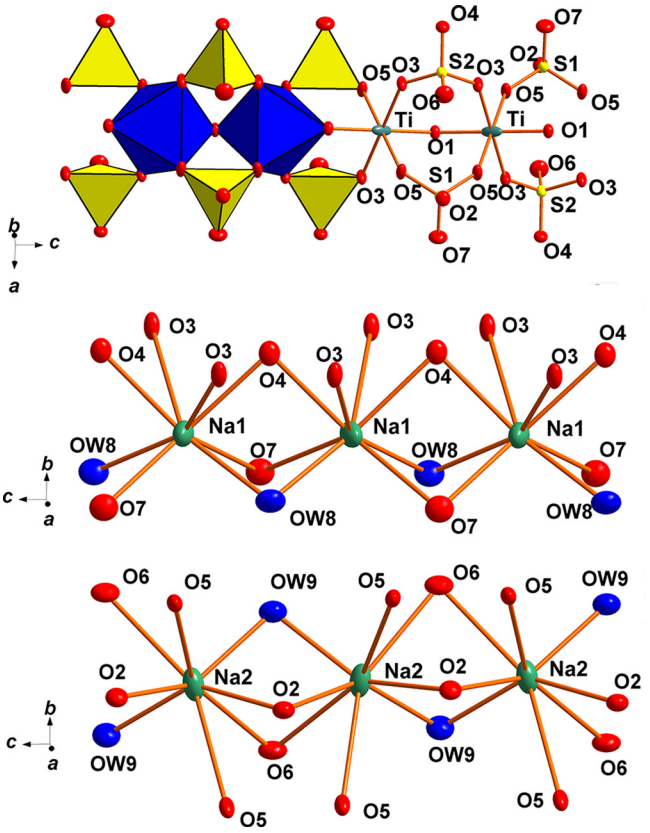

Fig. 4. (Top) $[TiO(SO_4)_2]$ chains consisting of TiO_6 octahedra and SO_4 tetrahedra; (bottom) coordination of Na atoms in the crystal structure of calamaite. Ellipsoids are drawn at 50% probability.

Calamaite represents a novel structure type. In its structure (Fig. 4) Ti^{4+} (with minor Fe^{3+} admixture) occupies an octahedrally coordinated site. The TiO_6 octahedra are interconnected *via* O(1) vertices to form infinite chains (Fig. 4). Minor amount of OH^- subsituting O^{2-} at the O(1) site is indicated by a relatively low bond-valence sum (Table 3). The $O_{0.95}H_{0.05}$ population of the O(1) site is given in agreement with the chemical data. The remaining vertices of the TiO_6 octahedron are shared with SO_4 tetrahedra thus forming one-dimensional $[TiO(SO_4)_2]$ units. Cohesion of $[TiO(SO_4)_2]$ units into a framework is provided *via* two crystallographically independent Na atoms: Na(1) and Na(2), which are both eight-coordinated by O atoms of SO_4 tetrahedra and H_2O molecules (Fig. 5). The SO_4 tetrahedra are distorted (Table 4), which is confirmed by the splitting of asymmetric stretching vibration bands in the IR spectrum of calamaite.

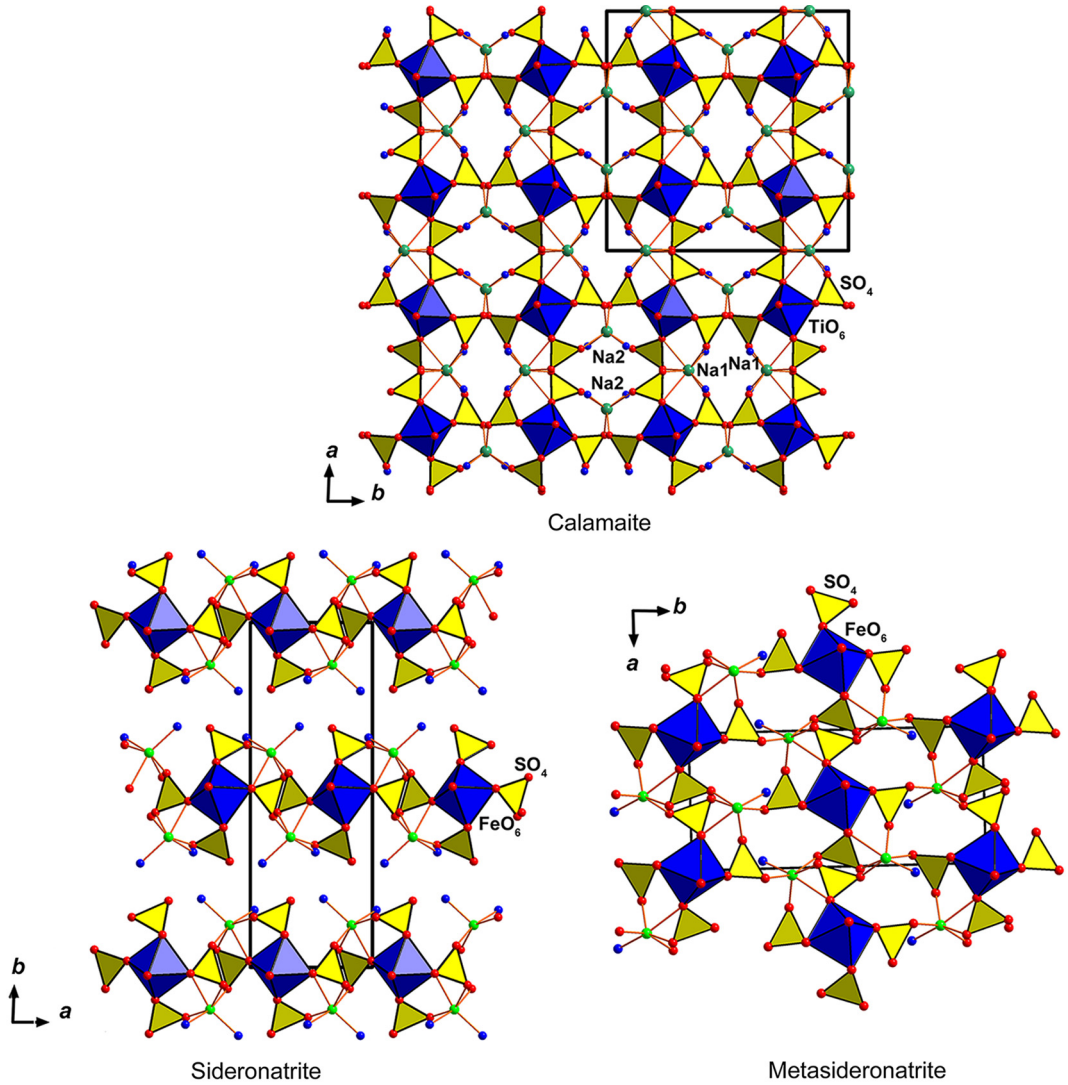

Fig. 5. (Top) General view of the crystal structure of calamaite [projection along the c axis, the unit cell is outlined; H_2O molecules are blue balls, Na atoms are green balls]; (bottom) heteropolyhedral chains topologically identical to those in calamaite but connected via NaO_n polyhedra to form layers in the structure of sideronatrite, $Na_2Fe^{3+}(OH)(SO_4)_2 \cdot 3H_2O$ (lower left; drawn based on data by Scordari & Ventruti, 2009). The same heteropolyhedral chains are interconnected via NaO_n polyhedra into framework in metasideronatrite, $Na_2Fe(SO_4)_2OH \cdot (H_2O)$ (lower right; drawn based on data by Ventruti *et al.*, 2010). Note: the heteropolyhedral chains in calamaite, sideronatrite and metasideronatrite run along the *c* axis.

The S–O bond-lengths with oxygen atoms shared with TiO_6 octahedra are slightly higher (1.49–1.50 Å) than other S–O distances (1.44–1.45 Å).

7. Discussion

Heteropolyhedral chains topologically identical to those in calamaite were previously described in sideronatrite, $Na_2Fe^{3+}(OH)(SO_4)_2 \cdot 3H_2O$ (Scordari & Ventruti, 2009), and metasideronatrite, $Na_2Fe^{3+}(OH)(SO_4)_2 \cdot H_2O$ (Ventruti *et al.*, 2010). However, in sideronatrite Na atoms connect these chains into layers (Fig. 5) further interconnected *via* hydrogen bonds only. In metasideronatrite the same heteropolyhedral chains are interconnected *via* NaO_n polyhedra into a framework topologically different from the above described framework in calamaite. The heteropolyhedral chains in calamaite, sideronatrite and metasideronatrite run along the *c* axis and these minerals have close values of the *c* unit-cell parameter: 7.01, 7.12 and 7.16 Å, respectively.

Unlike calamaite, octahedral sites in sideronatrite and metasideronatrite are occupied by Fe^{3+} only. In alcaparrosaite, $K_3(Ti^{4+}_{0.5}Fe^{3+}_{0.5})_2(SO_4)_4O{\cdot}2H_2O$, Ti^{4+} and Fe^{3+} occur in nearly equal amounts and are disordered at an octahedrally coordinated site, and the $(Ti_{0.5}Fe_{0.5})O_6$ octahedra are linked, sharing vertices, into dimers (Kampf *et al.*, 2012). Consequently, calamaite and alcaparrosaite are quite different in terms of structural topologies. Alcaparrosaite in its structural architecture is related to goldichite (Graeber & Rosenzweig, 1971). Other Ti^{4+} sulfates are known as synthetic compounds only (Gatehouse *et al.*, 1993).

Calamaite is the first sulfate mineral with a tetravalent cation octahedrally coordinated by O^{2-} but not OH^- anions, whereas natural sulfates with $M^{4+}(OH)_6$ octahedra (M^{4+} = Si, Ge, Mn, Sn) are known in two structurally related mineral groups. In the fleischerite group there are fleischerite $Pb_3Ge^{4+}(SO_4)_2(OH)_6 \cdot 3H_2O$ (Otto, 1975), schaurteite $Ca_3Ge^{4+}(SO_4)_2(OH)_6 \cdot 3H_2O$ (Origlieri & Downs, 2013), despujolsite $Ca_3Mn^{4+}(SO_4)_2(OH)_6 \cdot 3H_2O$ (Barkley *et al.*, 2011), and genplesite $Ca_3Sn^{4+}(SO_4)_2(OH)_6 \cdot 3H_2O$ (Pekov *et al.*, in press). In the ettringite group, the "pure" sulfate with $M^{4+}(OH)_6$ octahedra is only kottenheimite $Ca_3Si^{4+}(OH)_6(SO_4)_2 \cdot 12H_2O$ (Chukanov *et al.*, 2012), however, several carbonate-sulfates, borate-sulfates and sulfite-sulfates with $Si^{4+}(OH)_6$, $Ge^{4+}(OH)_6$ or $Mn^{4+}(OH)_6$ octahedra are known: see reviews in Pekov *et al.* (2012) and Chukanov *et al.* (2016b).

Calamaite is undoubtedly a supergene mineral formed in the oxidation zone of pyrite–quartz veins under conditions of abnormally arid climate that favours the preservation of the early, water-soluble sulfates, including species unstable in humid air. Mafic silicates of andesitic and dacitic host rocks dissolved by abundant sulfuric acid formed as a result of pyrite oxidation are the most probable source of Ti for calamaite and alcaparrosaite. The appearance of titanium sulfates indicates extremely high activity of natural sulfuric acid during the oxidation of pyrite ores at Alcaparrosa. Titanium, which is in nature usually almost immobile under low-temperature conditions, here demonstrates sufficient activity to form sulfates.

Acknowledgements: We thank Taras L. Panikorovskii and an anonymous referee for valuable comments. This study was supported by the Russian Science Foundation, grants nos. 14-17-00048 (electron microprobe and IR spectroscopic studies) and 16-17-10085 (X-ray diffraction studies and crystal structure determination). The technical support by the SPbSU X-Ray Diffraction Research Resource Center in the XRD studies is acknowledged.

References

Bandy, M.C. (1938): Mineralogy of three sulphate deposits of northern Chile. *Am. Mineral.*, **23**, 669–760.

Barkley, M.C., Yang, H., Evans, S.H., Downs, R.T., Origlieri, M.J. (2011): Redetermination of despujolsite, $Ca_3Mn^{4+}(SO_4)_2(OH)_6 \cdot 3H_2O$. *Acta Crystallogr.*, **E67**, i47–i48.

Brese, N.E. & O'Keeffe, M. (1991): Bond-valence parameters for solids. *Acta Crystallogr.*, **B47**, 192–197.

Britvin, S.N., Dolivo-Dobrovolsky, D.V., Krzhizhanovskaya, M.G. (2017): Software for processing the X-ray powder diffraction data obtained from the curved image plate detector of Rigaku RAXIS Rapid II diffractometer. *Zapiski RMO*, **146**, 104–107.

Bruker-AXS (2014): APEX2. Version 2014.11-0. Madison, Wisconsin, USA.

Chukanov, N.V., Britvin, S.N., Van, K.V., Möckel, S., Zadov, A.E. (2012): Kottenheimite, $Ca_3Si(OH)_6(SO_4)_2 \cdot 12H_2O$, a new ettringite-group mineral from the Eifel area, Germany. *Can. Mineral.*, **50**, 55–63.

Chukanov, N.V., Aksenov, S.M., Rastsvetaeva, R.K., Möhn, G., Rusakov, V.S., Pekov, I.V., Scholz, R., Eremina, T.A., Belakovskiy, D.I., Lorenz J.A. (2016a): Magnesiovoltaite, $K_2Mg_5Fe^{3+}{}_3Al(SO_4)_{12} \cdot 18H_2O$, a new mineral from the Alcaparrosa mine, Antofagasta region, Chile. *Eur. J. Mineral.*, **28**, 1005–1017.

Chukanov, N.V., Kasatkin, A.V., Zubkova, N.V., Britvin, S.N., Pautov, L.A., Pekov, I.V., Varlamov, D.A., Bychkova, Y.V., Loskutov, A.B., Novgorodova E.A. (2016b): Tatarinovite, $Ca_3Al(SO_4)[B(OH)_4](OH)_6 \cdot 12H_2O$, a new ettringite-group mineral from the Bazhenovskoe deposit, Middle Urals, Russia, and its crystal structure. *Geol. Ore Dep.*, **58**, 653–665 [translated from: Zapiski RMO, 145(1), 48–67 (in Russian)].

Gatehouse, B.M., Platts, S.N., Williams, T.B. (1993): Structure of anhydrous titanyl sulfate, titanyl sulfate monohydrate and prediction of a new structure. *Acta Crystallogr.*, **B49**, 428–435.

Graeber, E.J. & Rosenzweig, A. (1971): The crystal structures of yavapaiite, $KFe(SO_4)_2$, and goldichite, $KFe(SO_4)_2 \cdot 4H_2O$. *Am. Mineral.*, **56**, 1917–1933.

Kampf, A.R., Mills, S.J., Housley, R.M., Williams, P.A., Dini, M. (2012): Alcaparrosaite, $K_3Ti^{4+}Fe^{3+}(SO_4)_4O(H_2O)_2$, a new hydrophobic Ti^{4+} sulfate from Alcaparrosa, Chile. *Mineral. Mag.*, **76**, 851–861.

Marschik, R. & Fontboté, L. (2001): The Punta del Cobre Formation, Punta del Cobre-Candelaria area, northern Chile. *J. South Amer. Earth Sci.*, **14**, 401–433.

Origlieri, M.J. & Downs, R.T. (2013): Schaurteite, $Ca_3Ge(SO_4)_2(OH)_6 \cdot 3H_2O$. *Acta Crystallogr.*, **E67**, i6.

Otto, H.H. (1975): Die Kristallstruktur von Fleischerit, $Pb_3Ge[(OH)_6|(SO_4)_2] \cdot 3H_2O$, sowie kristallchemische Untersuchungen an isotypen Verbindungen. *N. Jb. Mineral. Abh.*, **123**, 160–190.

Palache, C., Berman, H., Frondel, C. (1951): The System of Mineralogy of James Dwight Dana and Edward Salisbury Dana, Yale University 1837–1892. 7th edition. Vol. II: Halides, Nitrates, Borates, Carbonates, Sulfates, Phosphates, Arsenates, Tungstates, Molybdates, etc. John Wiley & Sons, Inc., New York.

Pekov, I.V, Chukanov, N.V., Britvin, S.N., Kabalov, Y.K., Göttlicher, J., Yapaskurt, V.O, Zadov, A.E., Krivovichev, S.V., Schüller, W., Ternes, B. (2012): The sulfite anion in ettringite-group minerals: a new mineral species hielscherite, $Ca_3Si(OH)_6(SO_4)(SO_3) \cdot 11H_2O$, and the thaumasite-hielscherite solid-solution series. *Mineral. Mag.*, **76**, 1133–1152.

Pekov, I.V., Sereda, E.V., Zubkova, N.V., Yapaskurt, V.O., Chukanov, N.V., Britvin, S.N., Lykova, I.S., Pushcharovsky, D.Yu. (2018): Genplesite, $Ca_3Sn(SO_4)_2(OH)_6 \cdot 3H_2O$, a new mineral of the fleischerite group: first occurrence of a tin sulfate in nature. *Eur. J. Mineral.*, DOI:10.1127/ejm/2018/0030-2722. in press

Scordari, F. & Ventruti, G. (2009): Sideronatrite, $Na_2Fe(SO_4)_2(OH) \cdot 3(H_2O)$: crystal structure of the orthorhombic polytype and OD character analysis. *Am. Mineral.*, **94**, 1679–1686.

Sheldrick, G.M. (2015): New features added to the refinement program SHELXL since 2008 are described and explained. *Acta Crystallogr.*, **C71**, 3–8.

Ventruti, G., Stasi, F., Scordari, F. (2010): Metasideronatrite: crystal structure and its relation with sideronatrite. *Am. Mineral.*, **95**, 329–334.

Received 21 May 2017
Modified version received 10 August 2017
Accepted 30 August 2017